Comparative analysis of water adsorption capacity and cyclic stability of solvent-based and solvent-free MIL-101(Cr) for atmospheric water harvesting

Journal of Solid State Chemistry 359 (2026) 125972

Contents lists available at ScienceDirect

Journal of Solid State Chemistry

journal homepage: www.elsevier.com/locate/jssc

Comparative analysis of water adsorption capacity and cyclic stability of solvent-based and solvent-free MIL-101(Cr) for atmospheric water harvesting

Ranjeet Kumar [a], Syed Shabir Ahmed [a], Nadia Shahzad [a,*], Adeel Waqas [a], Naveed Hussain [b], Naseem Iqbal [a], Muhammad Imran Shahzad [c], Diego Pugliese [d,**]

[a] U.S.-Pakistan Center for Advanced Studies in Energy (USPCAS-E), National University of Sciences and Technology (NUST), H-12 Sector, Islamabad, 44000, Pakistan
[b] School of Photovoltaic and Renewable Energy Engineering (SPREE), University of New South Wales (UNSW), Sydney, 2033, Australia
[c] Nanosciences and Technology Department (NS&TD), National Center for Physics (NCP), Islamabad, 44000, Pakistan
[d] Division of Applied Metrology and Engineering, National Institute of Metrological Research (INRiM), 10135, Torino, Italy

ARTICLE INFO

Keywords:
Atmospheric water harvesting
Green synthesis
Metal–organic frameworks
Adsorption capacity
Cyclic stability
Sustainability

ABSTRACT

Water scarcity represents a major global challenge, affecting millions of people worldwide. Sorbent-based atmospheric water harvesting (SAWH) using metal–organic frameworks (MOFs) has emerged as a promising approach to mitigate this issue. However, the use of expensive and hazardous solvents in conventional MOF synthesis restricts large-scale applications. In this study, MIL-101(Cr) was synthesized through a solvent-free method, exhibiting high water adsorption capacity, rapid desorption behavior, and excellent cyclic stability, enabling solar-driven AWH across a broad range of relative humidity (RH). X-ray diffraction (XRD), scanning electron microscopy (SEM), and Brunauer–Emmett–Teller (BET) analyses confirmed the successful formation of solvent-free MIL-101(Cr) with a large specific surface area. The solvent-free material showed a 15% higher adsorption potential than its solvent-based counterpart, achieving a water uptake capacity of 0.547 g/g at 35% RH and 25 °C. 94.6% desorption was attained within 15 min at 70 °C, indicating suitability for low-energy, solar-thermal regeneration. Moreover, the green-synthesized material retained 93% of its adsorption capacity over 30 consecutive adsorption–desorption cycles. These findings demonstrate the potential of solvent-free MIL-101(Cr) as a cost-effective, durable, and sustainable sorbent for AWH applications.

1. Introduction

Water scarcity represents one of the most critical existential challenges faced by humanity [1]. According to a United Nations (UN) report, more than 3 billion people currently experience water scarcity worldwide, with the situation worsening particularly in arid and semi-arid regions [2,3]. Recent evidence [4] indicates that climate change–induced global warming and increasing precipitation variability are significantly intensifying the frequency and severity of droughts, particularly in arid and semi-arid regions. Under such conditions, groundwater remains a primary source of freshwater; however, its quality and long-term availability are increasingly threatened. For instance, a recent geographic information systems (GIS)-based assessment conducted in the semi-arid Marvdasht region of Iran revealed that soil composition and geological characteristics strongly influence groundwater salinity, with approximately 16% of the aquifer exhibiting electrical conductivity levels unsuitable for agricultural and drinking purposes [5]. Boretti et al. [6] further projected that more than two quarters of the global population may face an acute shortage of drinking water by 2050. Consequently, extensive research has been devoted to developing sustainable strategies to mitigate this crisis [7]. Among these, desalination has been widely adopted to convert saline water into potable water [8]. However, this approach is energy-intensive and requires significant initial investment, high operational costs, and proximity to seawater, which restricts its use primarily to coastal areas [9,10]. Membrane distillation has also been explored for the removal of toxic organic contaminants, such as toluene, from polluted water using hydrophobic polytetrafluoroethylene (PTFE) membranes [11].

* Corresponding author.
** Corresponding author.
E-mail addresses: nadia@uspcase.nust.edu.pk (N. Shahzad), d.pugliese@inrim.it (D. Pugliese).

https://doi.org/10.1016/j.jssc.2026.125972
Received 14 October 2025; Received in revised form 7 March 2026; Accepted 17 March 2026
Available online 19 March 2026

Nevertheless, this technique similarly requires considerable energy input and infrastructure investment. In parallel, advanced nanomaterials have been investigated for water remediation; for example, nano-ferrate(VI) has demonstrated effective oxidative degradation of aromatic dyes in both model and real water systems [12]. Despite their effectiveness in improving water quality, these treatment-based approaches do not directly generate new freshwater resources. This limitation underscores the urgent need for low-energy, decentralized technologies capable of supplementing conventional water supplies.

Atmospheric water harvesting (AWH) has emerged as a viable alternative, as it can be implemented in diverse geographical locations [13]. The atmosphere constitutes a vast reservoir of freshwater, containing approximately 13,000 trillion liters of water vapor—six times more than the freshwater present in Earth's rivers [14,15]. Unlike conventional water sources, atmospheric moisture is constantly renewed through evaporation and redistributed via large-scale atmospheric circulation and moisture transport processes [16]. Importantly, large-scale climatological analyses indicate that substantial amounts of water vapor persist even in arid and semi-arid regions, despite limited precipitation levels [17]. These findings highlight the atmosphere as a dynamically renewed and globally distributed freshwater source. The principal AWH techniques include dew-point condensation, fog collection, and sorbent-based atmospheric water harvesting (SAWH), each suitable under specific relative humidity (RH) conditions [18]. Dew-point condensation is often impractical in arid regions due to the substantial energy required to cool air below its dew point [19]. Similarly, fog collection depends on frequent dense fog and specific climatic conditions, which are uncommon in arid and semi-arid areas, limiting its reliability and cost-effectiveness [20]. In contrast, SAWH has gained considerable attention owing to its cost-effectiveness and efficient water capture in low-humidity environments. Nevertheless, its overall efficiency strongly depends on the properties of the sorbent material employed [14].

Physical sorbents, such as silica gels, exhibit limited water uptake due to low pore volumes, while zeolites require high regeneration temperatures resulting from strong interactions with water molecules, thus limiting their practical use [21,22]. Chemical sorbents, including lithium chloride, calcium chloride, and magnesium chloride, offer higher adsorption capacity and lower regeneration temperatures but suffer from deliquescence, leading to equipment corrosion and potential water contamination [23,24].

Metal–organic frameworks (MOFs) have recently attracted significant attention for SAWH applications due to their high porosity, tunable structure, and large specific surface area [25]. MOFs such as MIL-101 (Cr), MOF-303, and MIL-100(Fe) have demonstrated outstanding water stability, adjustable pore sizes, and excellent water adsorption performance [26]. In highly arid environments, materials such as MOF-303 and MOF-801 exhibit steep water uptake at low RH due to their strong hydrophilic affinity and well-defined adsorption sites. However, these frameworks typically display comparatively lower saturated adsorption capacities at moderate to high humidity levels. In contrast, MOFs characterized by larger pore volumes and higher total adsorption capacities are more suitable for operation across low-, mid-, and high-humidity conditions. Among these, MIL-101(Cr) stands out due to its exceptionally high surface area and large mesoporous cages, which enable substantial water uptake over a broad RH range [27]. This versatility makes MIL-101(Cr) particularly attractive for practical AWH applications under diverse climatic conditions. However, its conventional synthesis typically involves long reaction times and the use of costly and toxic solvents, limiting large-scale production [28]. Zhao et al. [29] investigated the regeneration behavior of MIL-101(Cr), reporting an equilibrium water uptake of 0.56 g/g at 25 °C and 50% RH, though the synthesis required prolonged reaction conditions (200 °C for 12 h), resulting in high fabrication costs. Similarly, Tan et al. [30] employed a mixed-solvothermal synthesis at 160 °C for 24 h using hydrofluoric acid (HF), achieving a water adsorption capacity of 0.921 g/g at 60% RH and 25 °C. Despite the high capacity, the extended reaction time and use of hazardous solvents such as HF restrict the practicality of this approach. These limitations underscore the urgent need for environmentally benign and scalable fabrication strategies for porous materials. Recent advances in green nanomaterial synthesis have demonstrated the feasibility of sustainable production routes without compromising functional performance. For example, a bio-hydrothermal approach has been reported for the construction of a $ZnFe_2O_4$/sub-5 nm NCS S-scheme heterostructure using plant extracts as mediating agents, highlighting the potential of eco-friendly synthesis pathways for advanced materials development [31]. Similarly, green or solvent-free synthesis strategies can be applied to MOFs to tailor structural and surface properties. Green-synthesized MOF-801, for instance, exhibited enhanced water adsorption compared to its solvothermal analogue, achieving a maximum uptake of 41.1 g/100 g at 25 °C and 80% RH, corresponding to a 12% increase in adsorption capacity. This improvement was attributed to increased defect density and the presence of additional hydrophilic functional groups [32]. Moreover, solvent-free synthesized MIL-100(Fe) has demonstrated superior adsorption capacity and stable cyclic performance for SAWH [33].

Although MIL-101(Cr) has been extensively studied for AWH applications, no research has yet explored the adsorption behavior of solvent-free synthesized MIL-101(Cr). To address this gap, the present study investigates the water adsorption performance of solvent-free MIL-101 (Cr) and compares it with that of hydrothermally synthesized MIL-101 (Cr). The structural and morphological characteristics of both samples were examined using advanced analytical techniques. Subsequently, their adsorption behavior was evaluated under varying RH conditions to assess the effects of temperature and RH on water uptake capacity. Desorption tests were conducted at different temperatures to determine regeneration efficiency, followed by cyclic adsorption–desorption experiments to evaluate long-term stability. As recently emphasized in the literature [34], multi-cycle AWH performance should be evaluated not only in terms of water generation rate but also considering effective sorbent utilization. Finally, the results were compared with previously reported studies. Through comprehensive evaluation of adsorption, desorption, and cyclic performance, this work provides valuable insights into the development of solvent-free MIL-101(Cr) as an efficient and sustainable sorbent for AWH.

2. Experimental section

2.1. Materials and chemicals

Chromium(III) nitrate nonahydrate, 1,4-benzenedicarboxylic acid (BDC), deionized (DI) water, anhydrous ethanol, and N,N-dimethylformamide (DMF) were purchased from Sigma-Aldrich with analytical-grade purity and used as received, without further purification.

2.2. Synthesis of MIL-101(Cr)

MIL-101(Cr) was synthesized using both solvent-based and solvent-free methods. The experimental conditions are summarized in Table 1.

For the solvent-based synthesis, MIL-101(Cr)(a) was prepared through a modified hydrothermal method following a previously

Table 1
Synthesis conditions of MIL-101(Cr) samples prepared by different methods.

S. no.	Sample name	Synthesis route	Crystallization time (h)	Temperature (°C)
1	MIL-101(Cr) (a)	Hydrothermal	8	220
2	MIL-101(Cr) (b)	Solvent-free	4	220

reported procedure [35], as illustrated in Fig. 1a. BDC (0.83 g) and chromium(III) nitrate nonahydrate (2 g) were dissolved in 25 mL of DI water and subjected to ultrasonication at 25 °C for 30 min. The resulting solution was then transferred to a Teflon-lined stainless-steel autoclave and heated to 220 °C at a ramp rate of 10 °C/min, followed by maintaining the temperature at 220 °C for 8 h to facilitate crystallization. The obtained product was collected by centrifugation at 10,000 rpm for 10 min and washed three times with ethanol and DMF to remove residual reactants. Finally, the purified material was dried in an oven at 120 °C for 12 h.

For the solvent-free synthesis, MIL-101(Cr)(b) was prepared according to a reported method [36] with minor modifications, as shown in Fig. 1b. Equimolar amounts (5 mmol each) of BDC and chromium(III) nitrate nonahydrate were mixed in a mortar and ground for 40 min at ambient conditions (25 °C, 40–60% RH) to ensure uniform blending. The resulting mixture was transferred to a Teflon-lined autoclave and heated to 220 °C at a ramp rate of 10 °C/min, followed by maintaining the temperature at 220 °C for 4 h. After cooling, the product was washed sequentially with DI water and hot ethanol (60 °C) to remove any unreacted precursors. The material was then centrifuged three times at 5500 rpm for 20 min to eliminate impurities and subsequently dried at 120 °C for 12 h.

2.3. Material characterization

The crystalline structure of the synthesized materials was analyzed by X-ray diffraction (XRD) using a Bruker D8 ADVANCE (Germany) diffractometer equipped with Cu Kα radiation ($\lambda = 1.5418$ Å) operating at 25 kV. The diffraction patterns were recorded in the 2θ range of 5°–90° with a step size of 0.02°. Surface morphology was examined using scanning electron microscopy (SEM, JSM-6490A, JEOL, Japan). Brunauer–Emmett–Teller (BET) surface area measurements were performed using a Quantachrome NovaWin 2.0 instrument (Virginia, USA) under a nitrogen atmosphere with a flow rate of 50 mL/min. Approximately 100 mg of each sample was gradually heated from room temperature prior to analysis to remove adsorbed moisture and gases.

2.4. Performance evaluation

Water adsorption experiments were conducted in a programmable temperature and humidity chamber (UTS E001, China). All samples were pre-dried at 140 °C for 2 h to ensure complete removal of moisture from the pores prior to testing. Subsequently, 1 g of each dried sample was used for the adsorption study. The mass change during adsorption was recorded using an electronic balance (BSM 420.3). The adsorption process is illustrated in Fig. 2a. Because the adsorption rate gradually decreased over time, the weighing interval was adjusted accordingly: data were recorded every 20 min during the first 2 h, every 30 min between 2 and 4 h, and every 60 min between 4 and 10 h. Adsorption equilibrium was considered achieved when the variation between two consecutive measurements was less than 3% over a 60-min interval. The adsorption capacity q (g/g) was calculated according to:

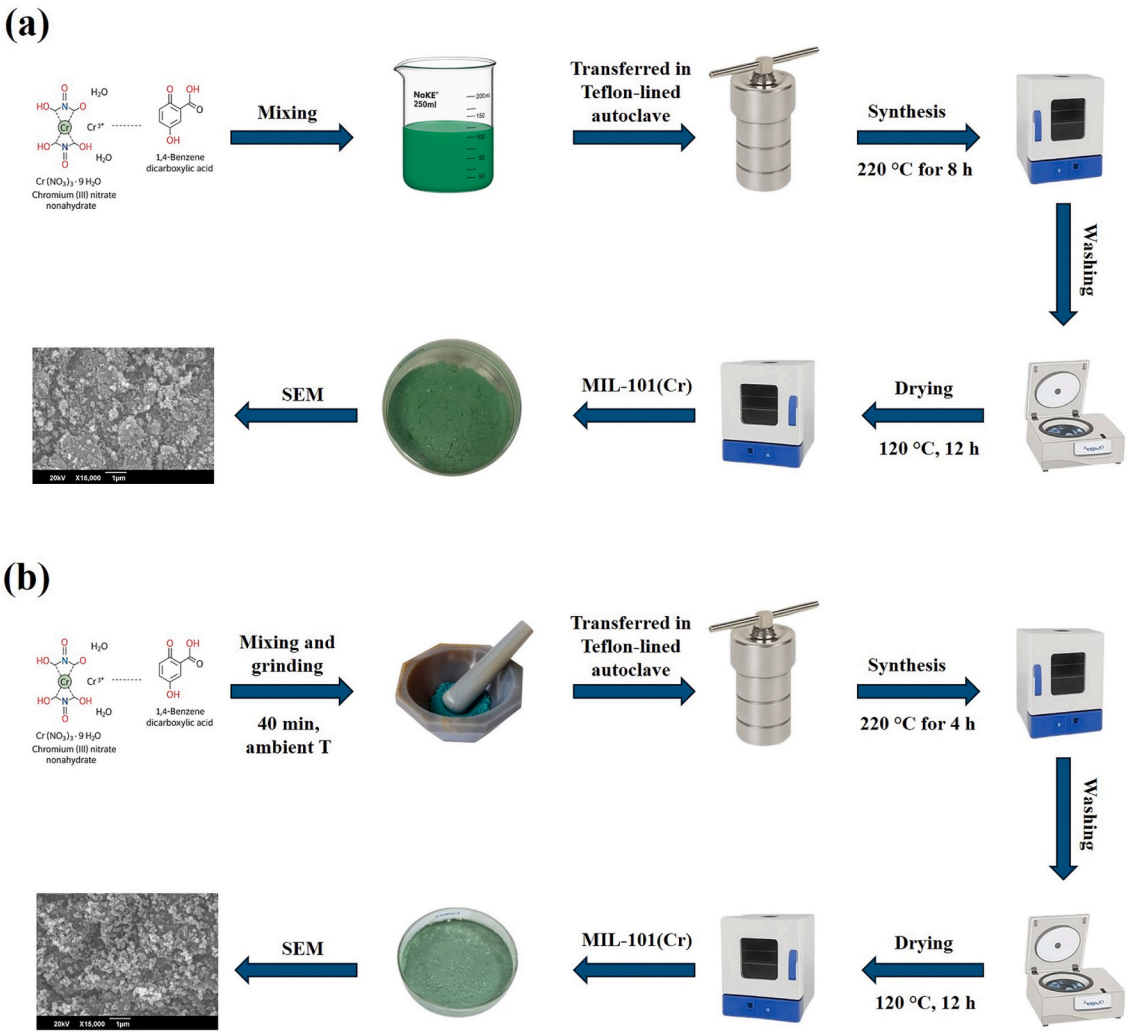

Fig. 1. Schematic illustration of MIL-101(Cr) synthesis via (a) solvent-based and (b) solvent-free routes.

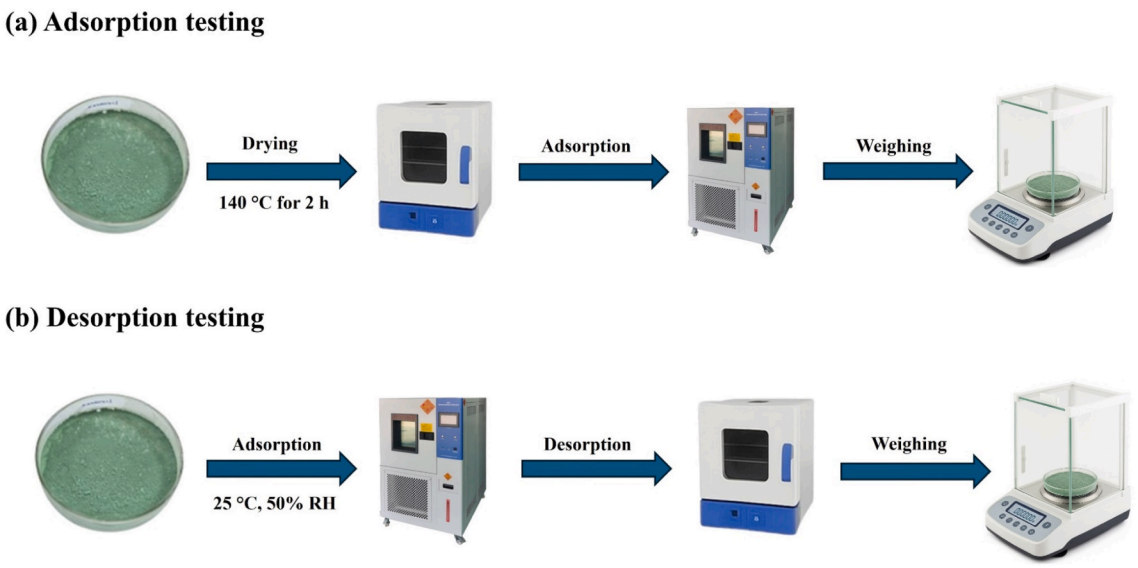

Fig. 2. Schematic representation of water (a) adsorption and (b) desorption testing procedures.

$$q = (m_f - m_i)/m_i$$

where m_i and m_f represent the initial and the final masses of the adsorbent before and after adsorption, respectively.

Desorption studies were performed in a temperature-controlled oven at various temperatures. Prior to testing, all samples were saturated under adsorption conditions at 25 °C and 50% RH. The sample mass was recorded every 5 min for a total duration of 60 min. The desorption efficiency η_{des} was calculated using the following equation:

$$\eta_{des} = \left(m_{des}/m_{ads}\right) \times 100$$

where m_{des} is the mass of water released during desorption and m_{ads} is the mass of water captured during adsorption. The complete desorption procedure is illustrated in Fig. 2b.

Cycling performance was evaluated by subjecting the samples to repeated adsorption–desorption cycles. Each sample was initially dried in a vacuum oven, followed by adsorption at 25 °C and 50% RH and desorption at 140 °C until a constant mass was achieved. This process was repeated 30 times, with the sample mass recorded at the beginning and end of each cycle to assess long-term stability.

3. Results and discussion

3.1. Characterizations

XRD, SEM, and BET analyses are widely employed to confirm the

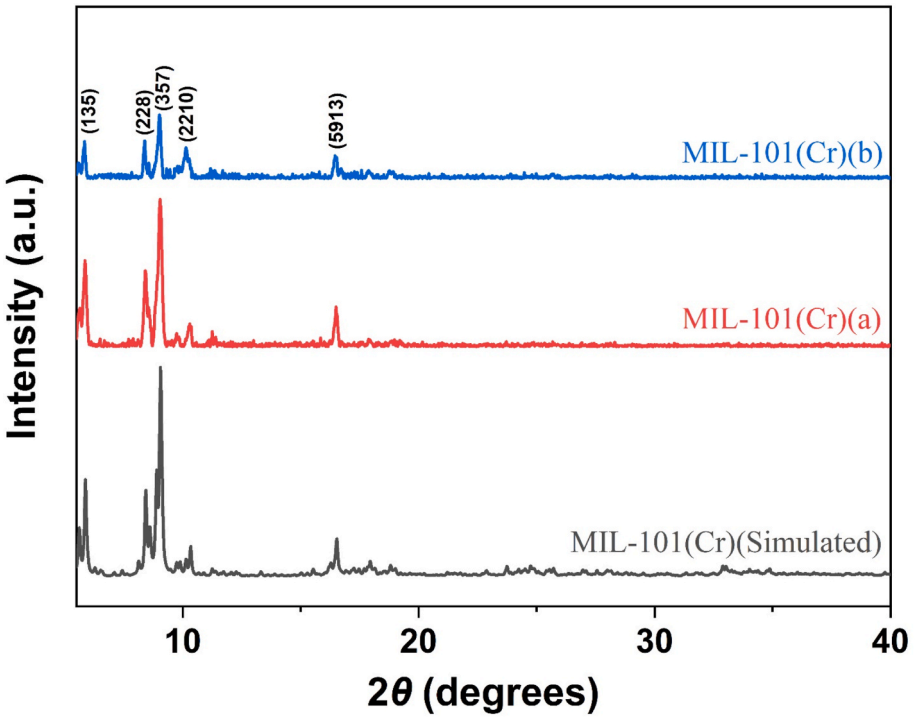

Fig. 3. Experimental XRD patterns of MIL-101(Cr)(a) and MIL-101(Cr)(b) compared with the simulated pattern from the reference structure.

structural integrity, crystallinity, morphology, and textural properties of MOF materials. For instance, these techniques have been successfully applied to characterize planar Cu-MOF and spherical Ni-MOF structures, verifying their coordination framework, morphology, and porosity [37]. In the present study, XRD analysis was performed to verify the crystal structure and phase purity of the synthesized materials. The diffraction peaks observed at 5.8°, 8.4°, 9.04°, 10.3°, and 16.5° correspond to the (135), (228), (357), (2210), and (5913) planes, in good agreement with previously reported data and with the simulated MIL-101(Cr) pattern derived from the crystallographic information file (CIF) card no. 400663 [38–40]. As illustrated in Fig. 3, the sharp and intense reflections of the solvent-based sample indicate the formation of highly crystalline MIL-101(Cr). In contrast, the broader peaks observed for the solvent-free sample suggest the presence of structural defects introduced during the solvent-free synthesis process [36]. Despite this, such defects can enhance water adsorption by providing additional active sites for water molecule interaction within the MOF framework [41].

SEM analysis further revealed pronounced morphological differences between the two materials, as shown in Fig. 4. The solvent-based MIL-101(Cr)(a) exhibited well-defined and uniform crystals, consistent with the high degree of crystallinity evidenced by XRD. Conversely, the solvent-free MIL-101(Cr)(b) displayed irregular particle shapes, indicative of structural imperfections and relatively lower crystallinity [36].

BET surface area analysis was conducted to evaluate the effect of synthesis conditions on the textural properties of the materials. The nitrogen adsorption–desorption isotherms (Fig. 5) exhibited characteristic type-I behavior typical of MIL-101(Cr), as previously reported [42]. The absence of hysteresis at high relative pressures confirmed the lack of meso- or macroporous structures [30]. The solvent-based MIL-101(Cr)(a) exhibited a slightly higher surface area (1948 m^2/g) compared with the solvent-free MIL-101(Cr)(b) (1876 m^2/g). The reduced surface area of the solvent-free material can be attributed to incomplete pore development and a lower degree of crystallinity [36,43].

3.2. Adsorption performance

Temperature plays a critical role in governing the adsorption capacity of sorbent materials, as it directly influences vapor pressure gradients, mass transfer kinetics, and adsorption–desorption equilibria. An increase in temperature can alter diffusion rates and modify the thermodynamic interactions between water molecules and active adsorption sites. The importance of temperature as a controlling environmental parameter has also been well documented in hydrological systems. For example, ambient temperature has been identified as a key predictor of dissolved oxygen levels among various water quality indicators [44], underscoring its fundamental influence on water-related processes. The adsorption performance of the sorbents was evaluated under controlled conditions at a constant RH of 50%, while the temperature was varied from 15 to 35 °C in increments of 10 °C. As shown in Fig. 6a, the adsorption capacity (q) of MIL-101(Cr)(a) increased with temperature, reaching 0.487 g/g at 15 °C and a maximum of 0.575 g/g at 25 °C. This behavior can be attributed to the higher kinetic energy of water molecules at elevated temperatures, which facilitates their diffusion into the sorbent pores [45]. However, a further temperature increase to 35 °C resulted in an initial rise in water uptake followed by a decline to 0.520 g/g, approximately 9% lower than the capacity at 25 °C. Although higher temperatures enhance molecular motion and diffusion, the accompanying increase in thermal energy weakens van der Waals interactions and hydrogen bonding between water molecules and the sorbent surface, leading to partial desorption and a reduced equilibrium capacity [46].

As illustrated in Fig. 6b, the solvent-free MIL-101(Cr)(b) exhibited its highest adsorption capacity at 25 °C, reaching 0.652 g/g—about 14% higher than the solvent-based counterpart. Across all tested temperatures, the solvent-free material consistently demonstrated superior water uptake, indicating its enhanced suitability for SAWH. Overall, temperature variation exerted only a moderate effect on adsorption performance, suggesting that MIL-101(Cr) materials are adaptable to a wide range of climatic conditions, including arid regions characterized by large diurnal temperature fluctuations.

RH is another critical parameter influencing the adsorption behavior of sorbent materials in SAWH systems [47]. To assess its effect, both samples were evaluated at a constant temperature of 25 °C under RH levels of 35, 50, 65, and 80%, as shown in Fig. 7. A clear positive correlation between RH and equilibrium water uptake was observed for both materials. This trend arises from the thermodynamic relationship between vapor pressure and adsorption potential: as RH increases, the partial pressure of water vapor rises, promoting capillary condensation within the porous framework of the sorbents [48].

The solvent-based MIL-101(Cr)(a) showed an adsorption capacity of 0.475 g/g at 35% RH, which increased to 0.685 g/g at 80% RH. In comparison, the solvent-free MIL-101(Cr)(b) exhibited a higher capacity of 0.547 g/g at 35% RH—about 15% greater than the solvent-based material—and reached 0.801 g/g at 80% RH. These results confirm the superior water adsorption performance of solvent-free synthesized MIL-101(Cr), highlighting its potential for efficient AWH, particularly in environments with variable humidity conditions.

3.3. Desorption performance

This study also examined the influence of temperature on the moisture-release kinetics of both samples. Prior to testing, the adsorbents were pre-conditioned at 25 °C and 50 % RH. Desorption experiments were then carried out in a temperature-controlled oven at 70–100 °C, with 10 °C increments.

Fig. 8 presents the desorption efficiency curves of solvent-based and

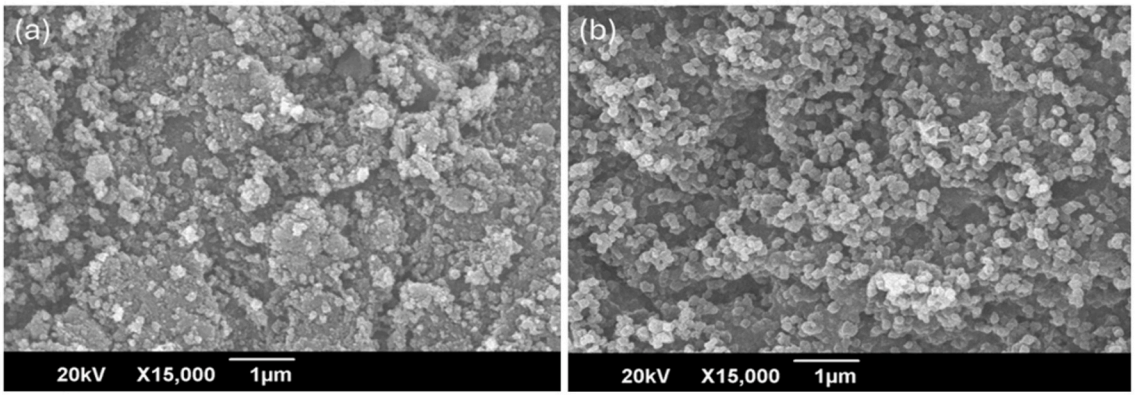

Fig. 4. SEM images of (a) solvent-based MIL-101(Cr)(a) and (b) solvent-free MIL-101(Cr)(b).

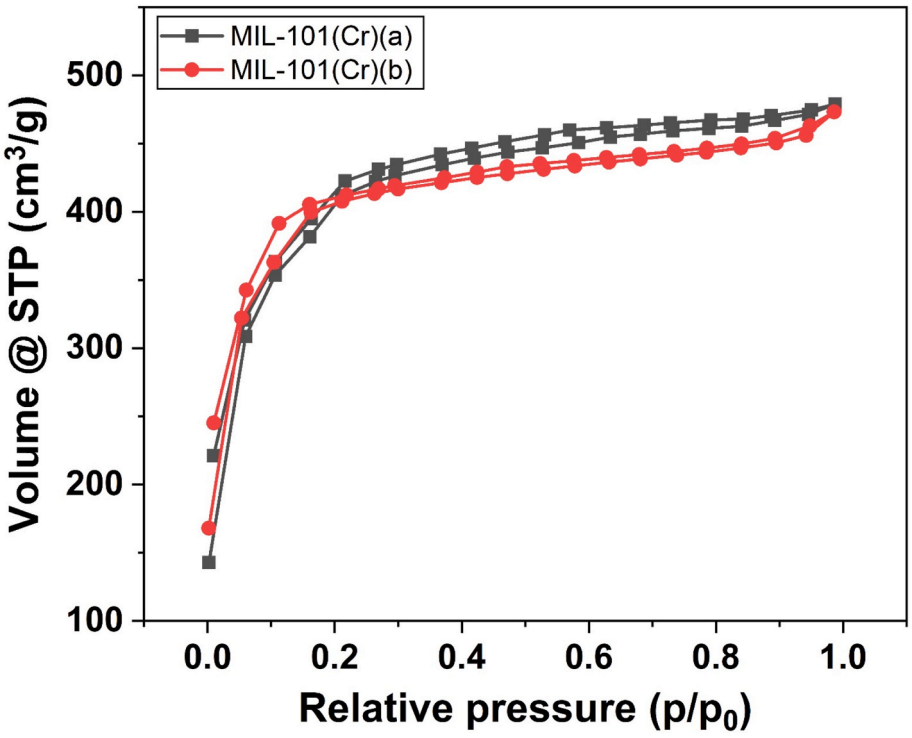

Fig. 5. N_2 adsorption/desorption isotherms of solvent-based and solvent-free MIL-101(Cr) samples.

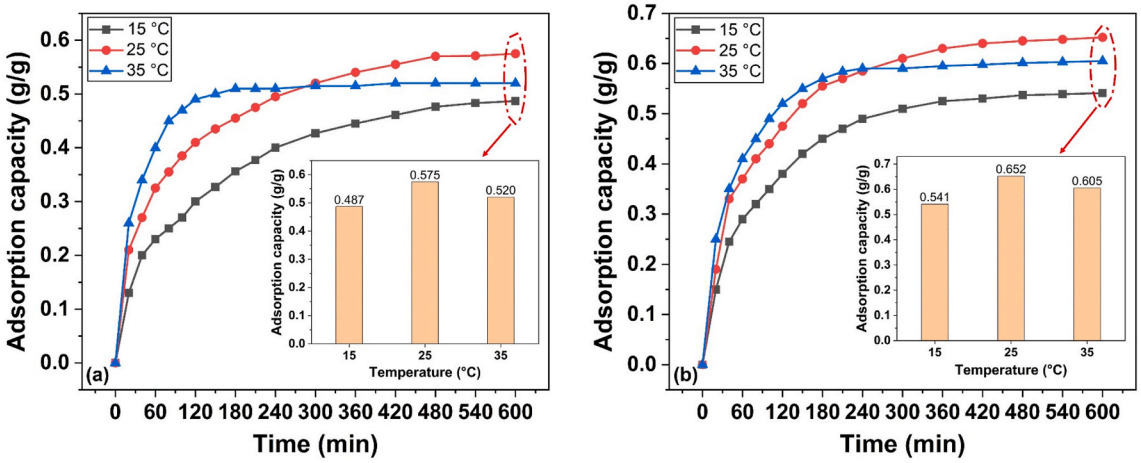

Fig. 6. Adsorption capacity of MIL-101(Cr) samples at 50% RH under three different temperatures: (a) solvent-based MIL-101(Cr)(a); (b) solvent-free MIL-101(Cr)(b). Insets show the maximum adsorption capacities for the three different temperatures.

solvent-free synthesized MIL-101(Cr). At the initial stage, both materials exhibited a rapid desorption response due to the removal of weakly bound water molecules, which require minimal energy to evaporate from the sorbent surface when heat is applied. The effect of temperature on desorption was clearly evident, as higher temperatures resulted in faster and more complete water release.

The solvent-free synthesized MIL-101(Cr) released 94.6%, 95.4%, 97.4%, and 98.5% of adsorbed water within 15 min, and 96.2%, 97.7%, 99.4%, and 99.9% within 25 min at 70, 80, 90, and 100 °C, respectively. In comparison, the solvent-based material desorbed 88.7%, 92.2%, 93.9%, and 95.6% within 15 min, and 94.8%, 96.5%, 99.1%, and 99.6% within 25 min under the same temperature conditions.

These results confirm that the solvent-free material exhibits superior desorption performance and can be efficiently regenerated at relatively low temperatures (≥70 °C), which can be readily supplied by solar-thermal energy.

3.4. Cyclic stability

Cyclic stability is a crucial performance indicator for assessing the long-term applicability of MOF-based materials in SAWH systems [49]. During repeated adsorption and desorption processes, interactions between water molecules and the metal clusters, or secondary building units (SBUs), may lead to partial ligand displacement, resulting in a gradual decline in adsorption capacity and structural degradation of the material [50,51]. Therefore, maintaining stable performance over multiple cycles is essential to ensure material durability.

The cyclic performance of the solvent-based and solvent-free MIL-101(Cr) samples was evaluated over 30 consecutive adsorption–desorption cycles at 25 °C and 50% RH, as illustrated in Fig. 9. Both

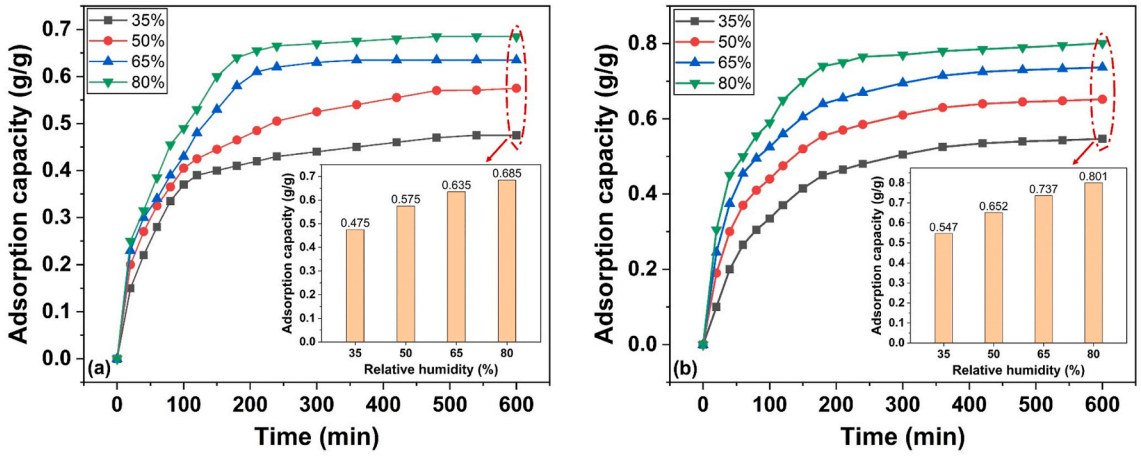

Fig. 7. Adsorption capacity of MIL-101(Cr)(a) and MIL-101(Cr)(b) at 25 °C under varying RH levels. Insets highlight the maximum adsorption capacities for the four tested RH conditions.

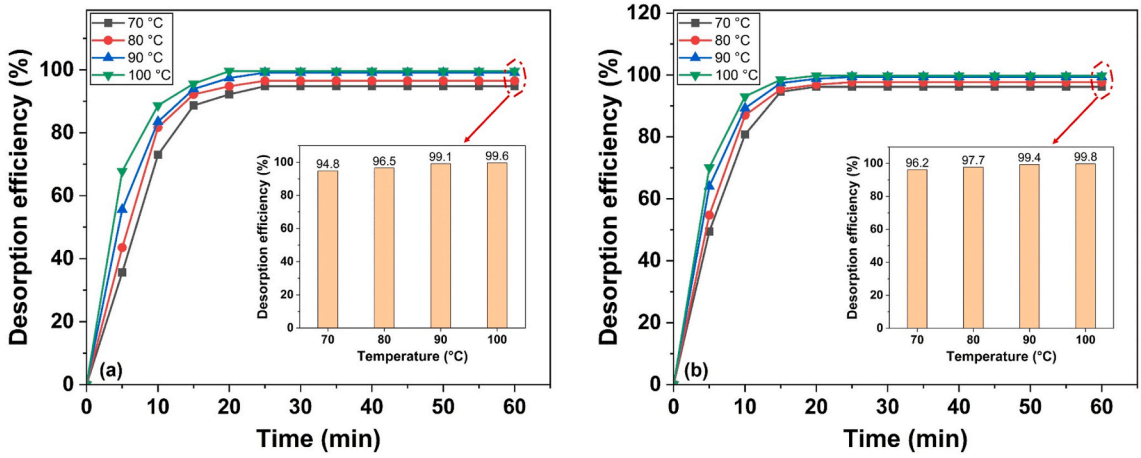

Fig. 8. Desorption efficiency of MIL-101(Cr) samples at different temperatures: (a) solvent-based MIL-101(Cr)(a); (b) solvent-free MIL-101(Cr)(b). Insets depict the maximum desorption efficiencies for the four tested temperatures.

samples exhibited a slight decrease in adsorption capacity with increasing cycle number; however, the solvent-free material consistently demonstrated higher water uptake than its solvent-based counterpart. This difference can be attributed to the structural defects generated during solvent-free synthesis, which provide additional active adsorption sites for water molecules [52]. After 30 cycles, the solvent-free MIL-101(Cr)(b) retained approximately 93% of its initial adsorption capacity, while the solvent-based MIL-101(Cr)(a) maintained 91%.

This stable performance over multiple cycles confirms that both materials possess good regeneration ability, with the solvent-free variant showing slightly enhanced cyclic durability. The visual appearance of the MIL-101(Cr) samples during adsorption and desorption is presented in Fig. 10. After adsorption at 50% RH and 25 °C, the material became noticeably darker in color (Fig. 10b). Following desorption (Fig. 10c), the original color was restored, and small droplets were observed on the surface, indicating the release of adsorbed water during the regeneration process.

4. Comparison with similar studies

A comparative analysis of water adsorption capacities reported for different MOF materials in the literature was performed, as summarized in Table 2. Most of these materials were synthesized using conventional solvothermal methods and evaluated under relatively high humidity conditions (typically above 40%) [53–55]. In contrast, the present work employed a solvent-free synthesis approach for MIL-101(Cr), thereby eliminating the use of solvents and reducing overall material cost and environmental impact.

Notably, the solvent-free synthesized MIL-101(Cr) demonstrated superior adsorption efficiency compared to its solvent-based counterpart. Furthermore, the material exhibited high and stable adsorption capacity even under low RH conditions, confirming its suitability for water harvesting applications in arid and semi-arid environments, where low RH represents a major limitation for most SAWH technologies.

5. Conclusions and future perspectives

MIL-101(Cr) was synthesized using both solvent-based and solvent-free methods, and its adsorption capacity, desorption behavior, and cyclic stability were systematically evaluated and compared. The solvent-free MIL-101(Cr) exhibited approximately 15% higher adsorption capacity at 35% RH and 25 °C than the solvent-based sample. In addition, the solvent-free material achieved rapid desorption at relatively low regeneration temperatures, releasing 94.6% of the adsorbed water within 15 min at 70 °C. This efficient desorption behavior highlights its potential for low-energy, solar-driven operation.

The solvent-free MIL-101(Cr) also demonstrated excellent structural

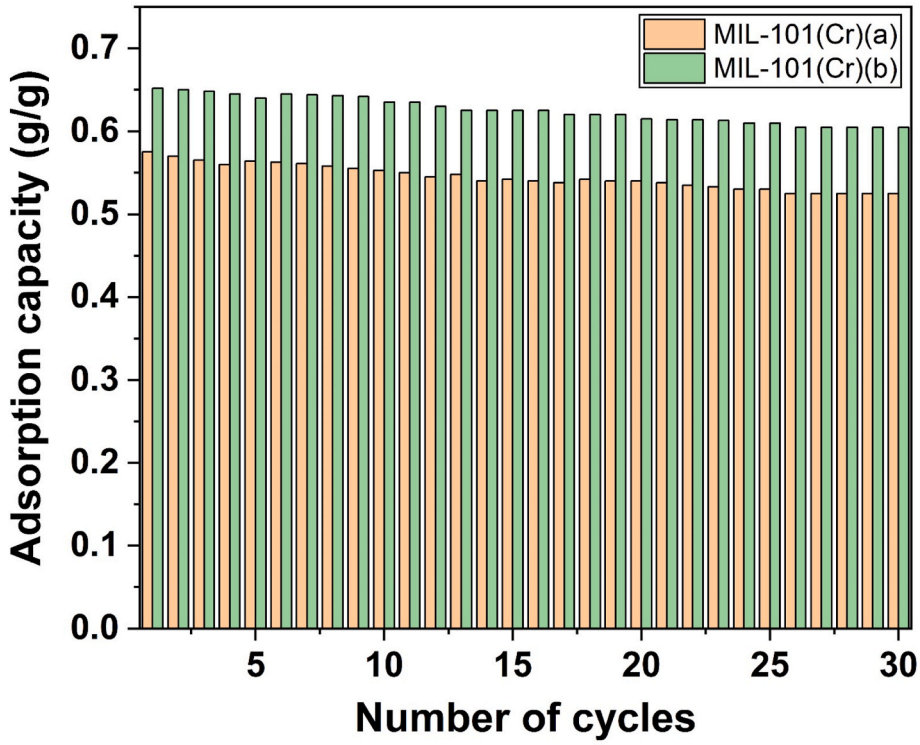

Fig. 9. Cyclic stability of solvent-based and solvent-free MIL-101(Cr) over 30 adsorption–desorption cycles.

Fig. 10. Visual changes in MIL-101(Cr) during the adsorption–desorption cycle: (a) dried powder before adsorption; (b) after adsorption at 50% RH and 25 °C; (c) after desorption showing condensed water droplets.

Table 2
Comparison of water adsorption capacities of solvent-free and solvent-based MIL-101(Cr) samples (this work) with other MOF materials reported in the literature.

MOF name	Synthesis technique	Adsorption capacity (g/g)	Relative humidity (%)	Temperature (°C)	Ref.
MIL-101(Cr)	Solvent-free	0.547	35	25	**This study**
		0.652	50		
		0.737	65		
		0.801	80		
MIL-101(Cr)	Hydrothermal	0.475	35	25	**This Study**
		0.575	50		
		0.635	65		
		0.685	80		
Ti-MIL-125	Solvothermal	0.429	50	22	[53]
UiO-66-NH_2	Solvothermal	0.394	50	22	[53]
MIL-101(Cr)	Solvothermal	0.223	50	22	[53]
PM NCM	Spray-electrospinning	0.22	50	25	[54]
MF@MIL-101(Cr)	Solvothermal	0.12	60	25	[55]

robustness, maintaining 93% of its original adsorption capacity after 30 consecutive adsorption–desorption cycles. These combined features—enhanced water uptake, fast regeneration, and strong cyclic stability—indicate that solvent-free MIL-101(Cr) is a promising and

cost-effective candidate for AWH applications.

Future investigations could focus on integrating MIL-101(Cr) with other functional materials such as graphene, hydrogels, polymers, hygroscopic salts, or nanoparticles to further improve its mechanical strength, adsorption efficiency, and desorption performance. The rational design of hybrid composites can improve interfacial compatibility, structural robustness, and long-term operational durability. For instance, the incorporation of a graphene oxide (GO)/Ni-MOF nanocarrier into an epoxy matrix has demonstrated pH-responsive controlled release behavior and enhanced protective performance through synergistic barrier and active (self-healing) mechanisms [56]. In parallel, the integration of advanced data-driven methodologies offers additional opportunities for system-level optimization. Hybrid modeling frameworks, such as the wavelet packet decomposition-sparrow search algorithm-fuzzy attention transformer (WPD-SSA-FAT) approach developed for nonlinear environmental systems [57], could be adapted to predict and optimize the real-time performance of MIL-101(Cr) under dynamic climatic conditions. Such strategies would support the development of intelligent, adaptive AWH systems with improved efficiency and operational resilience.

CRediT authorship contribution statement

Ranjeet Kumar: Writing – original draft, Visualization, Validation, Methodology, Investigation, Formal analysis, Data curation, Conceptualization. **Syed Shabir Ahmed:** Writing – original draft, Methodology, Investigation, Data curation, Conceptualization. **Nadia Shahzad:** Writing – review & editing, Validation, Supervision, Resources, Formal analysis, Conceptualization. **Adeel Waqas:** Writing – review & editing, Supervision. **Naveed Hussain:** Writing – review & editing. **Naseem Iqbal:** Writing – review & editing, Supervision. **Muhammad Imran Shahzad:** Writing – review & editing, Supervision. **Diego Pugliese:** Writing – review & editing, Visualization, Validation, Supervision.

Funding sources

This research did not receive any specific grant from funding agencies in the public, commercial, or non-profit sectors.

Declaration of competing interest

The authors declare that they have no known competing financial interests or personal relationships that could have appeared to influence the work reported in this paper.

Acknowledgments

The authors gratefully acknowledge the support of the Solar Energy Research Laboratory (SERL) at USPCAS-E, NUST, for providing the facilities and resources that made this research possible. Diego Pugliese acknowledges the support from the European Union—NextGenerationEU under the National Recovery and Resilience Plan (NRRP), Mission 04 Component 2 Investment 3.1|Project Code: IR0000027—CUP: B33C22000710006—iENTRANCE@ENL: Infrastructure for Energy TRAnsition aNd Circular Economy @EuroNanoLab.

Data availability

Data will be made available on request.

References

[1] G.T. Reader, Access to drinking water, food security and adequate housing: challenges for engineering, past, present and future, in: D.S.-K. Ting, A. Vasel-Be-Hagh (Eds.), Responsible Engineering and Living: Proceedings of Responsible Engineering and Living 2022 Symposium and Industry Summit (REAL2022), Springer, Cham, 2023, pp. 1–41.

[2] Summary progress update 2021: SDG 6 — water and sanitation for all | UN-Water. https://www.unwater.org/publications/summary-progress-update-2021-sdg-6-water-and-sanitation-all, 2021. (Accessed 12 December 2024).

[3] J.S. Shaikh, U. Aswalekar, S. Ismail, A. Akhade, The potential of integrating solar-powered membrane distillation with a humidification–dehumidification system to recover potable water from textile wastewater, Chem. Eng. Process. Process Intensif. 205 (2024) 110036, https://doi.org/10.1016/j.cep.2024.110036.

[4] Q. Zhang, W. Liu, P. Yue, L. Zhang, S. Wang, J. Yang, X. Lu, X. Yan, Discussion on major drought issues in the northern drought-prone belt in China, Bull. Am. Meteorol. Soc. 106 (2025) E678–E706, https://doi.org/10.1175/BAMS-D-24-0176.1.

[5] A. Azma, E. Narreie, A. Shojaaddini, N. Kianfar, R. Kiyanfar, S.M.S. Alizadeh, A. Davarpanah, Statistical modeling for spatial groundwater potential map based on GIS technique, Sustainability 13 (2021) 3788, https://doi.org/10.3390/su13073788.

[6] A. Boretti, L. Rosa, Reassessing the projections of the world water development report, npj Clean Water 2 (2019) 15, https://doi.org/10.1038/s41545-019-0039-9.

[7] H. Quon, S. Jiang, Decision making for implementing non-traditional water sources: a review of challenges and potential solutions, npj Clean Water 6 (2023) 56, https://doi.org/10.1038/s41545-023-00273-7.

[8] A. Panagopoulos, Brine management (saline water & wastewater effluents): sustainable utilization and resource recovery strategy through minimal and Zero Liquid Discharge (MLD & ZLD) desalination systems, Chem. Eng. Process. Process Intensif. 176 (2022) 108944, https://doi.org/10.1016/j.cep.2022.108944.

[9] I.C. Karagiannis, P.G. Soldatos, Water desalination cost literature: review and assessment, Desalination 223 (2008) 448–456, https://doi.org/10.1016/j.desal.2007.02.071.

[10] A. Feng, N. Akther, X. Duan, S. Peng, C. Onggowarsito, S. Mao, Q. Fu, S.D. Kolev, Recent development of atmospheric water harvesting materials: a review, ACS Mater. Au 2 (2022) 576–595, https://doi.org/10.1021/acsmaterialsau.2c00027.

[11] D. Gaur, K. Singh, S. Upadhyaya, Experimental study on the removal of toluene from water by PTFE hydrophobic microporous membrane using air gap membrane distillation process, Asian J. Water Environ. Pollut. 21 (2024) 77–85, https://doi.org/10.3233/AJW240037.

[12] A. Yaghoot-Nezhad, E. Saebnoori, I. Danaee, S. Elahi, N. Bahrami Panah, M. R. Khosravi-Nikou, Evaluation of the oxidative degradation of aromatic dyes by synthesized nano ferrate(VI) as a simple and effective treatment method, J. Water Process Eng. 49 (2022) 103017, https://doi.org/10.1016/j.jwpe.2022.103017.

[13] W. Chu, J. Ding, C. Peng, Z. Xu, Advancements in atmospheric water harvesting: toward continuous operation through mass transfer optimization, Commun. Eng. 3 (2024) 180, https://doi.org/10.1038/s44172-024-00324-y.

[14] Y. Zhong, L. Zhang, X. Li, B. El Fil, C.D. Díaz-Marín, A.C. Li, X. Liu, A. LaPotin, E. N. Wang, Bridging materials innovations to sorption-based atmospheric water harvesting devices, Nat. Rev. Mater. 9 (2024) 681–698, https://doi.org/10.1038/s41578-024-00665-2.

[15] J. Wang, W. Ying, L. Hua, H. Zhang, R. Wang, Global water yield strategy for metal-organic-framework-assisted atmospheric water harvesting, Cell Rep. Phys. Sci. 4 (2023) 101742, https://doi.org/10.1016/j.xcrp.2023.101742.

[16] Q. Wang, Y. Liu, G. Zhu, S. Lu, L. Chen, Y. Jiao, W. Li, W. Li, Y. Wang, Regional differences in the effects of atmospheric moisture residence time on precipitation isotopes over Eurasia, Atmos. Res. 314 (2025) 107813, https://doi.org/10.1016/j.atmosres.2024.107813.

[17] F.-F. Li, H.-L. Lu, G.-Q. Wang, J. Qiu, Long-term capturability of atmospheric water on a global scale, Water Resour. Res. 60 (2024), https://doi.org/10.1029/2023WR034757 e2023WR034757.

[18] H. Chen, T. Ran, Y. Gan, J. Zhou, Y. Zhang, L. Zhang, D. Zhang, L. Jiang, Ultrafast water harvesting and transport in hierarchical microchannels, Nat. Mater. 17 (2018) 935–942, https://doi.org/10.1038/s41563-018-0171-9.

[19] Y. Tu, R. Wang, Y. Zhang, J. Wang, Progress and expectation of atmospheric water harvesting, Joule 2 (2018) 1452–1475, https://doi.org/10.1016/j.joule.2018.07.015.

[20] H. Lu, W. Shi, Y. Guo, W. Guan, C. Lei, G. Yu, Materials engineering for atmospheric water harvesting: progress and perspectives, Adv. Mater. 34 (2022) 2110079, https://doi.org/10.1002/adma.202110079.

[21] N. Hanikel, M.S. Prévot, O.M. Yaghi, MOF water harvesters, Nat. Nanotechnol. 15 (2020) 348–355, https://doi.org/10.1038/s41565-020-0673-x.

[22] V. Baiju, P. Abhishek, K.L. Priya, S.P.A. Mohammed, Performance investigation of silica gel based consolidated composite adsorbents effective for adsorption desalination systems, Mater. Today Commun. 32 (2022) 104015, https://doi.org/10.1016/j.mtcomm.2022.104015.

[23] X.Y. Liu, W.W. Wang, S.T. Xie, Q.W. Pan, Performance characterization and application of composite adsorbent LiCl@ACFF for moisture harvesting, Sci. Rep. 11 (2021) 14412, https://doi.org/10.1038/s41598-021-93784-7.

[24] H. Qi, T. Wei, W. Zhao, B. Zhu, G. Liu, P. Wang, Z. Lin, X. Wang, X. Li, X. Zhang, J. Zhu, An interfacial solar-driven atmospheric water generator based on a liquid sorbent with simultaneous adsorption–desorption, Adv. Mater. 31 (2019) 1903378, https://doi.org/10.1002/adma.201903378.

[25] W. Xu, O.M. Yaghi, Metal-organic frameworks for water harvesting from air, anywhere, anytime, ACS Cent. Sci. 6 (2020) 1348–1354, https://doi.org/10.1021/acscentsci.0c00678.

[26] L.G. Gordeeva, M.V. Solovyeva, A. Sapienza, Y.I. Aristov, Potable water extraction from the atmosphere: potential of MOFs, Renew. Energy 148 (2020) 72–80, https://doi.org/10.1016/j.renene.2019.12.003.

[27] W. Chen, Y. Liu, B. Xu, B. Cheng, M. Ganesan, Y. Tan, M. Luo, B. Chen, X. Zhao, C. Lin, T. Qin, F. Luo, Y. Fang, S. Wang, X. Liang, W. Fu, B. Tan, R. Ye, D.Y. C. Leung, S.K. Ravi, Enhancing atmospheric water harvesting of MIL-101 (Cr) MOF

sorbent with rapid desorption enabled by Ni—Ni_3S_2 photothermal bridge, Adv. Funct. Mater. 34 (2024) 2410999, https://doi.org/10.1002/adfm.202410999.
[28] S. Ashraf, M. Sultan, M. Bahrami, C. McCague, M.W. Shahzad, M. Amani, R. R. Shamshiri, H.M. Ali, Recent progress on water vapor adsorption equilibrium by metal-organic frameworks for heat transformation applications, Int. Commun. Heat Mass Tran. 124 (2021) 105242, https://doi.org/10.1016/j.icheatmasstransfer.2021.105242.
[29] H. Zhao, Q. Li, Z. Wang, T. Wu, M. Zhang, Synthesis of MIL-101(Cr) and its water adsorption performance, Microporous Mesoporous Mater. 297 (2020) 110044, https://doi.org/10.1016/j.micromeso.2020.110044.
[30] B. Tan, Y. Luo, X. Liang, S. Wang, X. Gao, Z. Zhang, Y. Fang, Mixed-solvothermal synthesis of MIL-101(Cr) and its water adsorption/desorption performance, Ind. Eng. Chem. Res. 58 (2019) 2983–2990, https://doi.org/10.1021/acs.iecr.8b05243.
[31] K. Nateq, M. Shohani Zadeh, M. Amarzadeh, M. Rostami, I. Danaee, M.R. Khosravi-Nikou, In situ construction of green $ZnFe_2O_4$/sub-5nm N, Cu dual-doped SnO_2 S-scheme heterostructure with the boosted spatial charge separation towards decontamination of tetracycline: mechanistic perspectives and aquatic hazard assessment, J. Environ. Manag. 389 (2025) 126135, https://doi.org/10.1016/j.jenvman.2025.126135.
[32] M. Aghajani Hashjin, S. Zarshad, H.B. Motejadded Emrooz, S. Sadeghzadeh, Enhanced atmospheric water harvesting efficiency through green-synthesized MOF-801: a comparative study with solvothermal synthesis, Sci. Rep. 13 (2023) 16983, https://doi.org/10.1038/s41598-023-44367-1.
[33] H. Zhao, Q. Wang, Z. Xi, C. Liu, C. Miao, Experimental investigation on water vapor adsorption performance of solvent-free synthesized MIL-100(Fe) and its composite adsorbent, J. Solid State Chem. 324 (2023) 124135, https://doi.org/10.1016/j.jssc.2023.124135.
[34] J. Ding, M.R. Templeton, Y. He, C. Peng, W. Chu, Optimizing multi-cycle atmospheric water harvesting via sorbent utilization efficiency, Energy Environ. Sustainability. 1 (2025) 100025, https://doi.org/10.1016/j.eesus.2025.100025.
[35] Y. Hu, Z. Fang, X. Wan, X. Ma, S. Wang, S. Fan, M. Dong, Z. Ye, X. Peng, Carbon nanotubes decorated hollow metal–organic frameworks for efficient solar-driven atmospheric water harvesting, Chem. Eng. J. 430 (2022) 133086, https://doi.org/10.1016/j.cej.2021.133086.
[36] K. Leng, Y. Sun, X. Li, S. Sun, W. Xu, Rapid synthesis of metal–organic frameworks MIL-101(Cr) without the addition of solvent and hydrofluoric acid, Cryst. Growth Des. 16 (2016) 1168–1171, https://doi.org/10.1021/acs.cgd.5b01696.
[37] R. Majidi, A. Farhadi, I. Danaee, N. Bahrami Panah, D. Zarei, S. Nikmanesh, Investigation of synthesized planar Cu-MOF and spherical Ni-MOF nanofillers for improving the anti-corrosion performance of epoxy coatings, Prog. Org. Coat. 183 (2023) 107803, https://doi.org/10.1016/j.porgcoat.2023.107803.
[38] J. Yang, Q. Zhao, J. Li, J. Dong, Synthesis of metal–organic framework MIL-101 in TMAOH-$Cr(NO_3)_3$-H_2BDC-H_2O and its hydrogen-storage behavior, Microporous Mesoporous Mater. 130 (2010) 174–179, https://doi.org/10.1016/j.micromeso.2009.11.001.
[39] H. Chen, S. Chen, X. Yuan, Y. Zhang, Facile synthesis of metal-organic framework MIL-101 from 4-NIm–$Cr(NO_3)_3$–H_2BDC-H_2O, Mater. Lett. 100 (2013) 230–232, https://doi.org/10.1016/j.matlet.2013.03.053.
[40] S. Bhattacharjee, C. Chen, W.-S. Ahn, Chromium terephthalate metal–organic framework MIL-101: synthesis, functionalization, and applications for adsorption and catalysis, RSC Adv. 4 (2014) 52500–52525, https://doi.org/10.1039/C4RA11259H.
[41] S. Li, P. Wu, L. Chen, Y. Tang, Y. Zhang, L. Qin, X. Qin, H. Li, Enhanced atmospheric water harvesting (AWH) by Co-based MOF with abundant hydrophilic groups and open metal sites, J. Water Process Eng. 58 (2024) 104899, https://doi.org/10.1016/j.jwpe.2024.104899.
[42] C. Wang, S. Hou, M. Ma, Z. Ji, P. Wang, Y. Wang, Y. Su, Y. Zhou, M. Li, Recent development of MIL-101(Cr) for photocatalysis: a mini review, J. Water Process Eng. 66 (2024) 106040, https://doi.org/10.1016/j.jwpe.2024.106040.
[43] M. Zou, H. Zhu, M. Dong, T. Zhao, Template method for synthesizing hierarchically porous MIL-101(Cr) for efficient removal of large molecular dye, Materials 15 (2022) 5763, https://doi.org/10.3390/ma15165763.
[44] A. Azma, Y. Liu, M. Azma, M. Saadat, D. Zhang, J. Cho, S. Rezania, Hybrid machine learning models for prediction of daily dissolved oxygen, J. Water Process Eng. 54 (2023) 103957, https://doi.org/10.1016/j.jwpe.2023.103957.
[45] B. Zhang, Z. Zhu, X. Wang, X. Liu, F. Kapteijn, Water adsorption in MOFs: structures and applications, Adv. Funct. Mater. 34 (2024) 2304788, https://doi.org/10.1002/adfm.202304788.
[46] S. Fei, J. Gao, R. Matsuda, A. Endo, W.-L. Hsu, J.-J. Delaunay, H. Daiguji, Temperature effect on water adsorption and desorption processes in the mesoporous metal–organic framework MIL-101(Cr), J. Phys. Chem. C 126 (2022) 15538–15546, https://doi.org/10.1021/acs.jpcc.2c05603.
[47] E. Ansari, S. Elwadood, H. Balakrishnan, I. Sapkaite, C. Munro, G.N. Karanikolos, K. Askar, H. Arafat, S.S. Mao, L.F. Dumée, Sorption-based atmospheric water harvesters - perspectives on materials design and innovation, J. Environ. Chem. Eng. 12 (2024) 113960, https://doi.org/10.1016/j.jece.2024.113960.
[48] M. Ejeian, R.Z. Wang, Adsorption-based atmospheric water harvesting, Joule 5 (2021) 1678–1703, https://doi.org/10.1016/j.joule.2021.04.005.
[49] T.B. Čelič, A. Škrjanc, J.M. Coronado, T. Čendak, V.A. de la Peña O'Shea, D. P. Serrano, N. Zabukovec Logar, New insight into sorption cycling stability of three Al-based MOF materials in water vapour, Nanomaterials 12 (2022) 2092, https://doi.org/10.3390/nano12122092.
[50] Y. An, X. Lv, W. Jiang, L. Wang, Y. Shi, X. Hang, H. Pang, The stability of MOFs in aqueous solutions—research progress and prospects, Green Chem. Eng. 5 (2024) 187–204, https://doi.org/10.1016/j.gce.2023.07.004.
[51] M.J. Kalmutzki, N. Hanikel, O.M. Yaghi, Secondary building units as the turning point in the development of the reticular chemistry of MOFs, Sci. Adv. 4 (2018) eaat9180, https://doi.org/10.1126/sciadv.aat9180.
[52] H. Huang, Y. Heng, Z. Yu, X. Zhang, X. Zhu, Z. Fang, J. Li, X. Guo, Solvent-free synthesis of defective Zr-based metal–organic framework from waste plastic bottles for highly efficient lomefloxacin removal, J. Colloid Interface Sci. 670 (2024) 509–518, https://doi.org/10.1016/j.jcis.2024.05.125.
[53] M.W. Logan, S. Langevin, Z. Xia, Reversible atmospheric water harvesting using metal-organic frameworks, Sci. Rep. 10 (2020) 1492, https://doi.org/10.1038/s41598-020-58405-9.
[54] A. Li, J. Xiong, Y. Liu, L. Wang, X. Qin, J. Yu, A rapid-ab/desorption and portable photothermal MIL-101(Cr) nanofibrous composite membrane fabricated by spray-electrospinning for atmosphere water harvesting, Energy Environ. Mater. 6 (2023) e12254, https://doi.org/10.1002/eem2.12254.
[55] Y. Tao, Q. Li, Q. Wu, H. Li, Embedding metal foam into metal–organic framework monoliths for triggering a highly efficient release of adsorbed atmospheric water by localized eddy current heating, Mater. Horiz. 8 (2021) 1439–1445, https://doi.org/10.1039/D1MH00306B.
[56] R. Majidi, I. Danaee, L. Vrsalović, D. Zarei, Development of a smart anticorrosion epoxy coating containing a pH-sensitive GO/MOF nanocarrier loaded with 2-mercaptobenzothiazole corrosion inhibitor, Mater. Chem. Phys. 308 (2023) 128291, https://doi.org/10.1016/j.matchemphys.2023.128291.
[57] A. Azma, Y. Liu, S. Rezania, A hybrid WPD–SSA machine learning transformer for modeling nonlinear dynamics of flow systems, J. Water Process Eng. 82 (2026) 109448, https://doi.org/10.1016/j.jwpe.2026.109448.